Microscopy, 2022, **71(2)**, 124–131
DOI: https://doi.org/10.1093/jmicro/dfac005
Advance Access Publication Date: 14 February 2022
Article

MICROSCOPY

Serial ultrathin sections to identify ultrastructural localization of GLUT1 molecules in vesicles in brain endothelial cells—correlative light and electron microscopy in depth

Akane Yamada[1], Yoichiro Nishida[1], Kenjiro Wake[2], Ayako Nakamura[1], Yuriko Sakamaki[3], Hiroya Kuwahara[1], Toshiki Uchihara[1,4,*] and Takanori Yokota[1]

[1]Department of Neurology and Neurological Science, Graduate School of Medical and Dental Sciences, Tokyo Medical and Dental University, 1-5-45, Yushima, Bunkyo-ku, Tokyo 113-8519, Japan
[2]Liver Research Unit, Minophagen Pharmaceutical Co., Ltd., 3F., Shinjuku Mitsui Building No. 2, 3-2-11, Nishi-Shinjuku Shinjuku-ku, Tokyo 160-0023, Japan
[3]Microscopy Research Support Unit Research Core, Tokyo Medical and Dental University, 1-5-45, Yushima, Bunkyo-ku, Tokyo 113-8510, Japan
[4]Neurology Clinic with Neuromorphomics Laboratory, Nitobe Memorial Nakano General Hospital, 4-59-15, Chuo, Nakano-ku, Tokyo 164-8607, Japan
*To whom correspondence should be addressed. E-mail: uchihara@nakanosogo.or.jp

Abstract

Precise immunolocalization of molecules in relation to ultrastructural features is challenging, especially when the target is small and not frequent enough to be included in tiny ultrathin sections randomly selected for electron microscopy (EM). Glucose transporter 1 (GLUT1) is in charge of transporting glucose across brain capillary endothelial cells (BCECs). Paraformaldehyde-fixed floating sections (50 μm thick) of mouse brain were immunolabeled with anti-GLUT1 antibody and visualized with fluoronanogold. Fluorescent images encompassing the entire hemisphere were tiled to enable selection of GLUT1-positive BCECs suitable for subsequent EM and landmark placement with laser microdissection to guide trimming. Sections were then fixed with glutaraldehyde, gold enhanced to intensify the labeling and fixed with osmium tetroxide to facilitate ultrastructural recognition. Even though a region that contained target BCECs was successfully trimmed in the resin block, it was only after observation of serial ultrathin sections that GLUT1 signals in coated vesicles on the same cross section corresponding to the cross section preidentified by confocal laser microscope. This is the first ultrastructural demonstration of GLUT1 molecules in coated vesicles, which may well explain its functional relevance to transport glucose across BCECs. Successful ultrastructural localization of molecules in relation to well-preserved target structure in native tissue samples, as achieved in this study, will pave the way to understand the functional relevance of molecules and their relation to ultrastructural details.

Key words: blood–brain barrier, CLEM, coated vesicle, GLUT1, pre-embedding method, serial section

Introduction

Brain metabolism is exclusively dependent on glucose, whose supply to the brain is strictly controlled by the blood–brain barrier (BBB). Glucose transporter 1 (GLUT1) plays a major role in the regulation of glucose entry into the brain. It has been proposed that GLUT1 is internalized from the luminal membrane to the cytoplasm through endocytosis into brain capillary endothelial cells (BCECs) [1,2]. Among all transporters and receptors, GLUT1 is the most abundantly expressed in BCECs [3]. The localization of GLUT1 in brain tissue has been reported on the luminal and abluminal membrane and cytoplasm of BCECs [4–6]. Although association of GLUT1 molecule with endosome was suspected on cultured cells [7], its precise topology associated with vesicular structures in the cytoplasm remains to be clarified. Immunolabeling intensity is compromised after standard tissue processing for EM with glutaraldehyde fixation followed by embedding in epoxy resin [8]. Embedding in hydrophilic resin, LR white, may theoretically improve immunolabeling [9], while ultrastructural details are not always sufficient to visualize the GLUT1 in relation to membrane and vesicular structures [5]. Therefore, how to maximize immunolabeling intensity while maintaining ultrastructural integrity has been the major issue in immunoelectron microscopy (immunoEM). In our previous studies [10,11], initial immunolabeling of formalin-fixed tissue with fluorescent nanocrystals, Quantum Dots (QDs) allowed precise selection of target based on the fluorescent signal of QDs. It was possible to trim the section and to fix it again with glutaraldehyde and osmium tetroxide so that structural details are well preserved, wherein QD labeling is identifiable as electron-dense particles. This dual visibility of QDs, fluorescence and electron density, allowed direct comparison of immunofluorescence and immunoEM images of the same target as comparative light and electron microscopy

Received 28 September 2021; Revised 10 January 2022; Editorial Decision 20 January 2022; Accepted 4 February 2022

Table 1. List of materials used for immunostaining in this study

Name	Immunogen structure	Host	Manufacturer	Cat#	Type	Dilution
Anti-GLUT1 antibody	Rat GLUT1 AA 481 to 492	Rabbit	Abcam	ab14683	polyclonal	1:2500
GLUT1 peptide	Human GLUT1 AA 450 to 492	Human	Abcam	ab202335	–	1:20 (mol)
Anti-rabbit HRP	Rabbit IgG	Goat	Abcam	ab7090	polyclonal	1:1000
Biotinated anti-rabbit IgG	Rabbit IgG	Goat	Vector	PK-6101	polyclonal	1:1000
Alexa Fluor 488 FluoroNanogold-Fab'anti-rabbit antibody	–	–	Nanoprobes	#7204	–	1:200

AA, amino acid; GLUT1, glucose transporter 1.

(CLEM). This two-step CLEM approach, as we established previously, is particularly useful to identify infrequent targets on fluorescent microscopy followed by immunoEM counterpart of the same target. Fluoronanogold is also equipped with similar dual visibility by conjugating nanogold particles with fluorochrome [12]. Fluoronanogold may be superior to QDs because EM visibility of nanogold particles could be enhanced after exposure to gold solution [13]. In the present study, GLUT1-positive fluorescent signals from fluoronanogold were used to select GLUT1-positive BCECs suitable for subsequent preparation for EM observation [10]. Even if a region containing target BCECs was successfully trimmed in the resin block, an additional step to obtain serial ultrathin sections was necessary to visualize small and infrequent GLUT1 molecules. With this novel strategy of three-step CLEM, we identified precise localization of GLUT1 molecules in a well-preserved background in mouse brain.

Materials and methods

C57BL/6 mice (female; 6 weeks old) were obtained from Charles River Laboratories Japan, Inc. (Yokohama, Japan). All protocols were approved by the ethics committee of Tokyo Medical and Dental University.

Tissue processing for immunohistochemistry

Following anesthesia with isoflurane, the mice were perfused transcardially with 0.1 M phosphate buffer (PB; pH 7.4) for 5 min and then ice-cold 4% paraformaldehyde in 0.1 M PB for 10 min. Brains were immersed in 4% paraformaldehyde in 0.1 M PB overnight. Serial coronal brain sections (50 µm thick) were prepared by using a vibrating blade microtome (VT1000 S, Leica, Inc., Wetzlar, Germany).

Characterization of anti-GLUT1 antibody

The antibodies and peptide used in this study are shown in Table 1. The antibodies recognized the amino acid (AA) sequence of GLUT1 from AA 481 to 492 (C-terminus), which are 100% identical among human, mouse and rat. Fresh mouse brain tissue was dissected for use in western blot analysis and frozen at −80°C. The frozen brain cortex was homogenized in 100 µl of buffer (10 mM Tris-HCL, pH 7.4, containing 150 mM NaCl, 1 mM ethylenediaminetetraacetic acid (EDTA), 4% 3-[(3-cholamidopropyl)dimethylammonio]-1-propanesulfonate hydrate) with a tablet of protease inhibitor cocktail (Roche Ltd., Basel, Switzerland, Cat# 11697498001), and then spun at 100 000 × *g* for 20 min at 4°C. The protein concentration in the supernatant was then determined by using a Pierce BCA protein assay kit (Thermo Scientific, Tokyo, Japan, Cat# 23225). Samples were denatured at 95°C for 5 min and then subjected to 10% polyacrylamide gel electrophoresis. Proteins in the gel were transferred onto a polyvinylidene difluoride membrane (Sequi-Blot, Cat# 162-0184, Bio-Rad Laboratories Inc., CA, USA). After being blocked with 5% skimmed milk in Tris-buffered saline (50 mM Tris-HCl, pH 7.5, 150 mM NaCl), the membranes were incubated for 1 h at room temperature with rabbit anti-GLUT1 antibody (1:1000; Abcam, Cambridge, UK, Cat# ab14683) or the equivalent diluted antibody that had been incubated overnight at 4°C with a 20× molar excess of GLUT1 peptide (Abcam, Cambridge, UK, Cat# ab202335). Then, the membranes were incubated with an appropriate horseradish peroxidase–conjugated secondary antibody (1:1000; Abcam, Cambridge, UK, Cat# ab7090) (Fig. 1).

For the immunohistochemical study, 50-µm-thick floating sections were pretreated with 1% orthoperiodic acid for 15 min at room temperature. The sections were washed with 0.1 M PB, incubated with 0.3% hydrogen peroxide in 0.1 M PB (pH 7.4) for 30 min and blocked with 5% normal goat serum—0.05% NaN_3 in 0.1 M PB (pH 7.4) for 30 min. They were then incubated with the rabbit anti-GLUT1 antibody (1:1000) at 4°C for 2 days. In a parallel experiment, the anti-GLUT1 antibody solution was coincubated with a 20× molar excess of the GLUT1 peptide before use. The sections were subsequently incubated with biotinylated secondary anti-rabbit antibody (1:1000; Vector Laboratories Inc., CA, USA, Cat# PK-6101) for 2 h. After incubation of the sections with streptavidin–peroxidase complex (1:1000; Vector Laboratories Inc., CA, USA, Cat# PK-6101) for 1 h, color development was performed with 0.01% diaminobenzidine, 0.01% nickel ammonium chloride, 0.5% imidazole and 0.04% hydrogen peroxide in 0.05 M Tris-HCl buffer. Sections were mounted with Entellan new (Merck, Darmstadt, Germany, Cat#107961) and examined by light microscopy (BX53, Olympus Corporation, Tokyo, Japan) (Fig. 2).

GLUT1 immunostaining with fluoronanogold

Sections were pretreated with 1% orthoperiodic acid for 15 min at room temperature and washed with 0.1 M PB. They were then incubated with 5% normal goat serum in PB (pH 7.4) for 30 min, rabbit anti-GLUT1 antibody

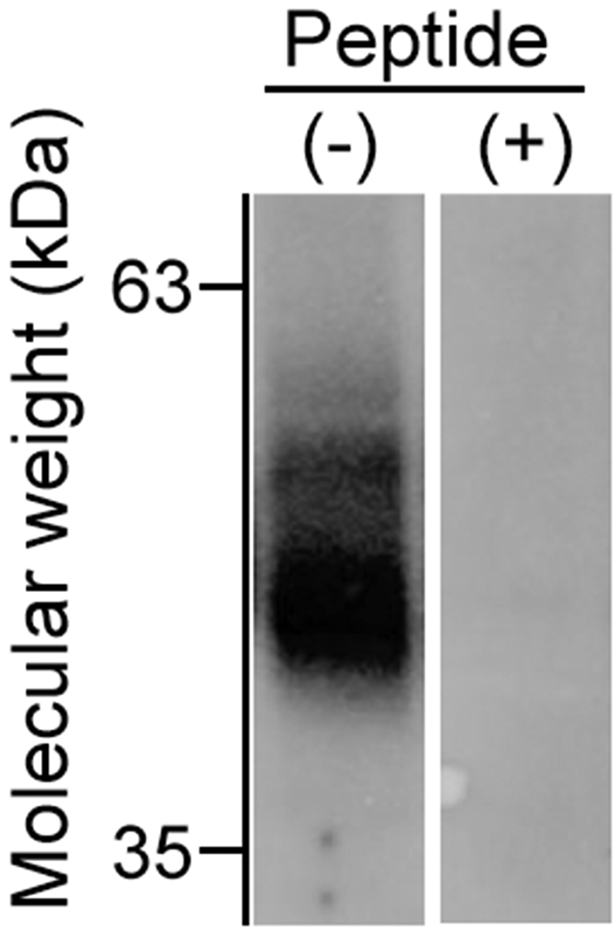

Fig. 1. Pre-absorption test of polyclonal anti-GLUT1 antibody by western blot analysis. The GLUT1 band was strongly detected in normal mouse brain lysate with anti-GLUT1 antibody (left lane). The band was not detected after pre-incubation of the anti-GLUT1 antibody with GLUT1 peptide (right lane).

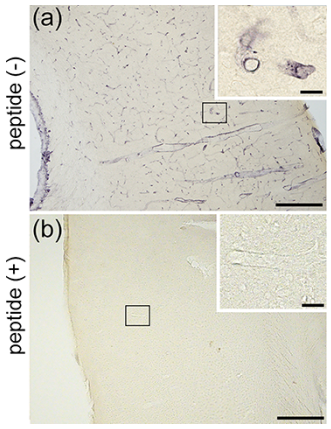

Fig. 2. Pre-absorption test of anti-GLUT1 antibody by immunohistochemistry. (a) Capillary vessel walls in a mouse brain were stained with the antibody. (b) Intensity of the GLUT1 immunostaining in the capillary was greatly decreased after pre-incubation with GLUT1 peptide. The inset images are a higher magnification of the rectangles in the main image. Scale bars = 50 μm in main image; 5 μm in inset image.

(1:200 or 1:5000) at 4°C for 2 days and secondary Alexa Fluor 488 FluoroNanogold-Fab′ anti-rabbit antibody (1:200; Nanoprobes Inc., NY, USA, Cat# 7204) at 4°C for 2 days. Sections were mounted with mounting medium containing 4′,6-diamidino-2-phenylindole (DAPI) (Vector Laboratories Inc., CA, USA, H-1200).

Whole-slide mapping of the fluorescent GLUT1 signal

To pinpoint GLUT1-positive BCECs for immunoEM, we conducted whole-slide mapping of the fluorescent GLUT1 signal. We captured 288 snapshots of each section by using a light microscope with transmitted light (data not shown) and with two fluorescence channels (for GLUT1 and DAPI signals); the integrated image of the 288 snapshots after the subtraction of overlapping areas was 0.136 mm^2. Schematics of the image before and after integration of the snapshots are shown in Fig. 3a and b; the integrated image was 14 901 × 16 778 pixels at 0.4 μm/pixel. The fluorescent signals from GLUT1/AlexaFluor 488 FluoroNanogold and from DAPI were excited by a laser unit (LU4A, Nikon Corp., Tokyo, Japan). Signals were captured through fluorescent filters (450/50 MHE57010 and 525/50 MHE57030, Nikon Corp., Tokyo, Japan) with peak excitation wavelength of 488 and 405 nm, respectively, by using an electron multiplying charge-coupled device camera (DU-897, Andor, Belfast, UK) connected to a microscope (Eclipse Ti microscope, Nikon Corp., Tokyo, Japan) (Fig. 3a). Because random sampling of brain tissue for immunoEM may fail to retrieve GLUT1-positive BCECs, whole-slide mapping of the fluorescent GLUT1 signal was used to select target cells as candidates for EM preparation. To locate all the GLUT1-positive signals in the entire section, at various positions (XY plane) and depths (Z axis), a motorized stage connected to the microscope was driven by NIS-Elements software (version 4.50, Nikon Corp., Tokyo, Japan). Dozens of points in the section were assigned appropriate XYZ coordinates by the software. Snapshots at specific depths were captured with the motorized stage by using the assigned Z coordinate values; if a snapshot did not have an assigned Z coordinate value, it was captured by using the median Z coordinate value of the snapshots surrounding it. If a large snapshot were taken to cover the whole hemisphere, some parts of the snapshot would be out of focus, whereas other parts would be in focus. To avoid this problem, 288 serial in-focus snapshots of the fluorescent image were obtained with a 40× objective (Plan Apo λ, Nikon Corp., Tokyo, Japan) and tiled to generate a single seamless image of 14 901 pixels × 16 778 pixels at a resolution of 0.4 μm/pixel (Fig. 3b) [11]. A 5.96 × 6.71 mm transmitted light image with all parts in focus was obtained. It took 15 min to tile the entire hemisphere for bright field images and 30 min for fluorescent images. This whole-slide mapping allowed us to select candidate BCECs that could be used to obtain cross sections for immunoEM. The candidate BCECs were chosen by the criteria of intense GLUT1 signals and orientation perpendicular to the section surface. Next, we set a 1.2-mm square region of interest (ROI) in the cerebral cortex and captured 6069 snapshots by confocal laser scanning microscopy (CLSM). The ROI containing these BCECs was captured by the same microscope equipped with a confocal system (A1R Nikon Corp, Tokyo, Japan) with a 40× objective lens (Plan Apo λ, Nikon Corp., Tokyo, Japan); this Z-stack scan yielded a three-dimensional (3D) data set of

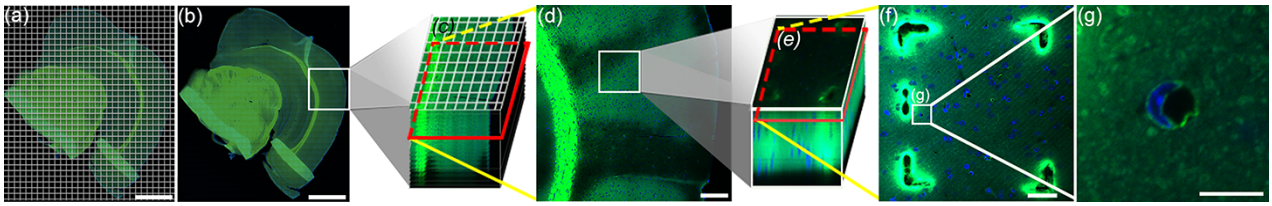

Fig. 3. Successive steps for obtaining fluorescent immunostained microscopic images of the GLUT1 signal in a cross section of a capillary in a mouse cerebral cortex. (a) Snapshots captured with a 40× objective lens were tiled to cover the entire hemisphere. Scale bar = 1 mm. (b) A region of interest (ROI; white square) was set in the integrated light image (14 901 × 16 778 pixels, 0.4 μm/pixel). Scale bar = 1 mm. (c) CLSM images of the ROI with 21 XY planes at 1-μm intervals were simultaneously captured. (d) One CLSM image including a cross section of a BCEC was chosen, and this BCEC cross-section was set as a new square ROI (0.262 μm/pixel, 4622 × 4622 pixels). Scale bar = 200 μm. (e) After laser marking, CLSM images of the new ROI with 44 XY planes at 1-μm intervals were obtained. (f) A single optical section including the target BCEC cross section and laser marking is shown. Scale bar = 50 μm. (g) A representative CLSM image of a BCEC cross section is shown. Scale bar = 10 μm. The green fluorescence represents anti-GLUT1 antibody/Alexa Fluor 488 FluoroNanogold-Fab' anti-Rabbit IgG, whereas the blue represents 4′,6-diamidino-2-phenylindole (DAPI; a marker of nuclear DNA).

21 XY planes at 1-μm intervals with each plane covered by 289 snapshots in two fluorescence channels (Fig. 3c). Each image was 4622 × 4622 pixels at 0.262 μm/pixel (Fig. 3d). The total file size was 1.7 GB. About 6 h was required to capture this 3D data set. These tomographic images enabled us to identify a confocal cross section (Fig. 3d) that included BCEC cross sections suitable for EM observation.

Ultrastructural mapping of GLUT1

To facilitate the recognition of 3D-reconstructed GLUT1-positive BCECs for use as targets in immunoEM, a 250-μm square area containing multiple BCEC cross sections was defined in the cortex, and landmarks were punched out around the target BCECs with the use of a laser microdissection instrument (LMD7000, Leica, Inc., Wetzlar, Germany). These landmarks were used to guide subsequent trimming of the section. Then a Z-stack scan of the target BCECs was re-performed by CLSM with a 40× objective lens; images (1024 pixels × 1024 pixels at 0.262 μm/pixel; total data set size, 176.5 MB) were produced at 1-μm intervals over a total depth of 44 μm (Fig. 3e). The reason for re-imaging with CLSM was that the position of the target cell shifts by several tens of micrometers when its XY coordinates are identified by the fluorescence microscope attached to the laser microdissection instrument. This shift is due to the difference in resolution between fluorescence microscopy and CLSM. A representative region surrounded by the landmarks is shown in Fig. 3f. Next, cross-sectional images of the target BCECs (1024 × 1024 pixels at 0.1 μm/pixel) were captured with a 100× oil immersion objective lens (Plan Apo VC, Nikon Corp., Tokyo, Japan) at 1-μm intervals across an average total depth of 6 μm (Fig. 3g). Cross sections of individual BCECs that contained a nucleus and were thus suitable for EM observation were captured by CLSM (Fig. 3g).

To obtain the target BCECs on EM, the section was detached from the glass slide and fixed in 2% glutaraldehyde for 10 min. After being washed with 0.1 M PB, the section was incubated in gold enhancement solution (Nanoprobes Inc., NY, USA, Cat# 2114) for 5 min to increase the visibility of nanogold labeling for immunoEM. The section was rewashed with 0.1 M PB and fixed in 1% osmium tetroxide for 30 min. It was then dehydrated in a series of graded ethanol solutions, equilibrated with propylene oxide 3 times for 15 min, and incubated with resin-containing solution, propylene oxide:epoxy resin (1:1), for 1 h. The section was incubated with 100% pure resin for 2 h at room temperature. To produce an epon-embedded specimen with flat surfaces, the section was gently pressed between Aclar films (Nissin EM, Tokyo, Japan, Cat# 4513) and hardened with heat (60°C) in an oven for 48 h. Under a stereomicroscope, the section was first trimmed to 2 mm in diameter under the guidance of the landmarks in the GLUT1-positive BCEC 3D map constructed by confocal microscopy, and the Aclar film on one side was detached from the hardened epon-embedded section. The section was then stuck to columnar epon that had been prepared in advance and trimmed again with the guidance of the landmarks. Serial ultrathin sections (80 nm thick) were obtained by using an ultramicrotome (EM UC7, Leica, Inc., Wetzlar, Germany) and manually collected on copper grids. The grids were stained with uranyl acetate and lead citrate and then observed with a JEM-1400 flash transmission electron microscope (JEOL, Tokyo, Japan). Besides GLUT1 signals, about 100 coated vesicles and 20 uncoated ones were also observed in BCECs by immunoEM.

Results

Immunological characterization of anti-GLUT1 antibody

First, the specificity of anti-GLUT1 antibody was assessed by western blot analysis by using normal mouse brain lysate. The polyclonal anti-GLUT1 antibody identified a main band between 35 and 63 kDa that approximately corresponded to the molecular weight of GLUT1 (Fig. 1). The broad band seen in the blots results from heterogeneous glycosylation of GLUT1 [14]. The band was not detected when the anti-GLUT1 antibody had been pre-incubated with the GLUT1 peptide. Next, in the immunohistochemical study of normal mouse brain tissue, many capillary walls were clearly identified in the cortex by the anti-GLUT1 antibody (Fig. 2a); this was as expected from the abundance of GLUT1 in BCECs [14]. When the anti-GLUT1 antibody was pre-incubated with the GLUT1 peptide, the intensity of the capillary wall immunostaining was greatly decreased (Fig. 2b).

The immunoEM counterpart of GLUT1 demonstrated its accumulation around BCEC cytoplasmic membrane as expected. Its ultrastructural localization was different according to the concentration of the primary antibody (0, 1:200 or 1:5000) as shown in Fig. 4. In the negative control, the signals were absent (Fig. 4a and d). At 1:200, GLUT1-positive particles were found on the luminal membrane and in the cytoplasm of BCEC (Fig. 4b and e) as previously reported [4,5,15]. These GLUT1 signals on the abluminal membrane were not frequent at 1:5000, while those in the cytoplasm are clearly highlighted (Fig. 4c and f).

Serial ultrathin sections to visualize GLUT1 labeling in trimmed BCECs

CLSM cannot reveal the ultrastructural localization of GLUT1 molecules in the cytoplasm of the target BCECs owing to the low resolution and the diffraction of the fluorescent GLUT1 signal (Fig. 5a). Whereas the original floating section is 50 μm thick and each optical slice for CLSM is estimated to be 2.18 μm thick, each final ultrathin section for EM spans only 80 nm (Fig. 5b and c). Therefore, it is necessary to obtain serial ultrathin sections to visualize enhanced nanogold labeling of GLUT1. This serial approach demonstrated that ultrastructural localization of GLUT1 labeling varied from

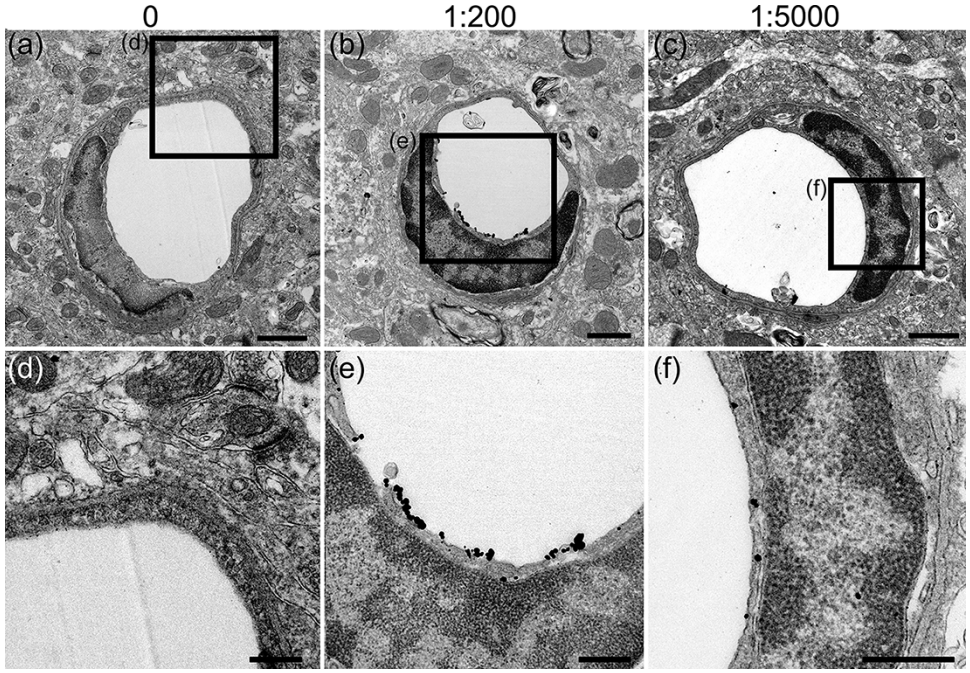

Fig. 4. Effect of anti-GLUT1 antibody concentration on the amount of immunoEM signals. Without the primary antibody, GLUT1 signals were rarely observed (a, d). Electron micrograph showed that, at higher primary antibody concentration, labeling of GLUT1 appeared to be enhanced on the luminal side of BCECs (b, e). On the other hand, at a lower primary antibody concentration, labeling appeared to be confined to the cytoplasm and plasma membrane of BCECs. Scale bars = 1 μm in (a–c), 500 nm in (d–f).

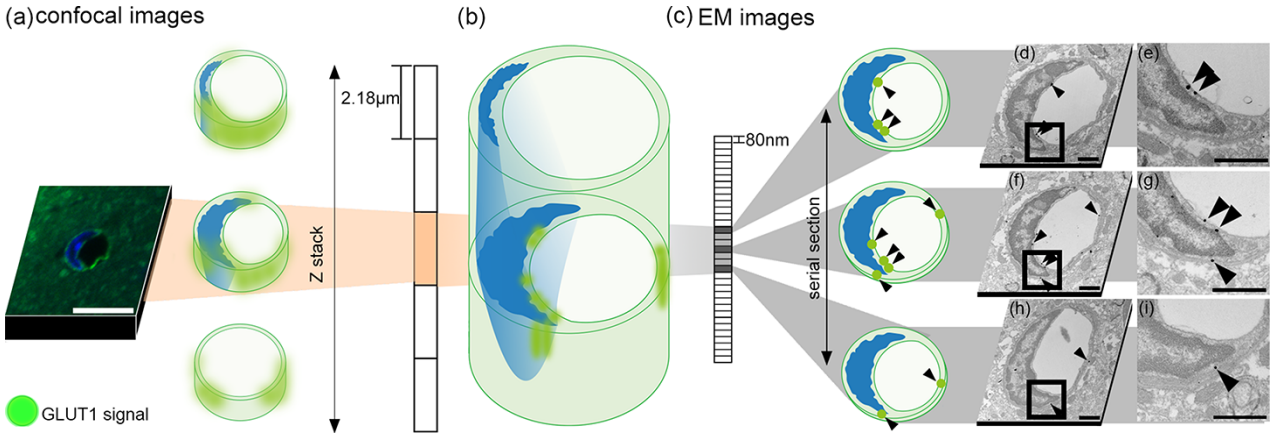

Fig. 5. Detection of GLUT1 molecules by light microscopy and transmission electron microscopy. (a) An optical section (2.18 μm thick) was acquired by CLSM, as shown in Fig. 3g. The section contained nucleus (blue) and GLUT1 (green) signals. Scale bar = 10 μm. (b) GLUT1 fluorescence signal spreading in the Z direction in a capillary vessel is illustrated. (c) Serial sections (80 nm thick) of the optical section were obtained. (d–i) Electron microscopic images of a capillary cross section showed GLUT1 molecules in the blood capillary endothelial cells (arrowheads). Each panel shows a different serial section; the sections displayed are not consecutive. Scale bars = 1 μm. (e, g, i) Higher magnification of the squares in (d, f, h). Scale bars = 1 μm.

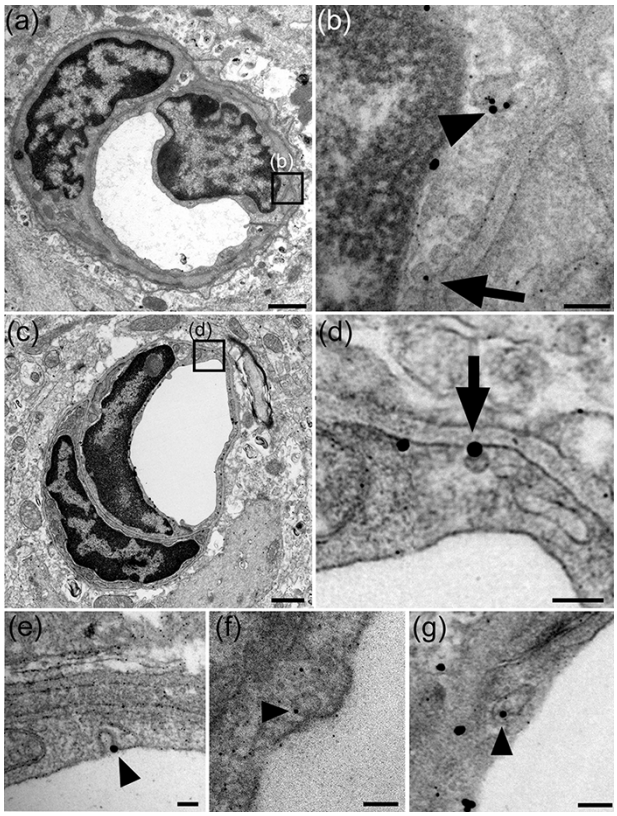

Fig. 6. Transmission electron microscopy images of a BCEC cross section. (a, c) Representative whole cross-sectional views of a BCEC are shown. Scale bar = 1 μm. (b, d) Higher magnification of the square in (a) and (c). Gold particle signals representing GLUT1 are localized in the intracellular vesicle (arrowhead) and on the abluminal cellular membrane (arrows). Scale bar = 100 nm. (e–g) GLUT1 signals in (e) an open vesicle on the luminal side, (f) a closed vesicle on the luminal side and (g) a medium-sized vesicle are shown. Scale bar = 100 nm.

one section to another (Fig. 5d–i, arrowheads) and that the corresponding fluorescent signal (green, Fig. 5a) was their summation. We succeeded in demonstrating GLUT1 signals with clear surrounding structures (Fig. 6).

Discussion

The resolution of CLSM is too low to reveal the subcellular localization of GLUT1 in BCECs. Even on an immunoEM image with much higher resolution, the membrane structure cannot be observed with the post-embedding method in a hydrophilic resin, such as LR white [6,9,16–18]. To overcome this problem, we developed the pre-embedding method described above for immunoEM, and we here demonstrated the detection of GLUT1 molecules while successfully preserving ultrastructural detail in BCECs in mouse brain. Usually, ultrastructural details are best preserved when glutaraldehyde-fixed samples are embedded in epoxy resin. Because this standard approach leads to the deterioration of antigenicity of almost all epitopes, it is difficult to obtain strong immunolabeling if the antibodies are applied after embedding the sample in epoxy resin (post-embedding approach). In our protocol, brain tissue was perfused with paraformaldehyde and immunolabeled with the anti-GLUT1 antibody before being embedded in epoxy resin (pre-embedding approach). By fluorescence microscopy, we confirmed the well-preserved epitope antigenicity of GLUT1 immunolabeled with fluoronanogold (Fig. 3). This fluorescent signal was useful to identify appropriate BCECs for subsequent trimming for EM. Because GLUT1 labeling can be heterogeneous and BCECs are variously oriented (Fig. 2a), it was sometimes difficult to hit appropriate BCECs (strong labeling and oriented perpendicularly to the section surface) if trimming is performed randomly without guidance. To identify best possible candidate BCECs for subsequent immunoEM, overlapping fluorescent images were captured and tiled to encompass the entire hemisphere. After landmarking appropriate BCECs (Fig. 3f), we were able to perform post-fixation with glutaraldehyde and osmium tetroxide to preserve ultrastructural details and conduct gold enhancement to enhance GLUT1 labeling. Although initial fixation with paraformaldehyde is not ideal for preservation of ultrastructural details, immunolabeling was more efficient before post-fixation with glutaraldehyde and osmium tetroxide, which preserved ultrastructural details (Fig. 6). We were, however, initially disappointed to find that the initial ultrathin sections did not contain GLUT1-positive signals. Even though the initial ultrathin sections did not contain GLUT1-positive signals, it was quite sure that the trimmed resin block, which motivated us to obtain serial ultrathin sections until appropriate sections containing GLUT1 signals are obtained. A previous study used serial ultrathin sectioning and the CLEM method to identify target structures as small as a dendritic spine [19]. Although obtaining serial ultrathin sections is laborious work that requires skill and concentration, hundreds of ultrathin sections were sufficient to obtain sections with GLUT1 labeling (Fig. 5). Our results indicate that serial ultrathin sections are necessary to demonstrate small targets such as GLUT1 molecules, which have an estimated diameter of only 6 nm and are scattered in BCECs [20]. In contrast, conventional random sampling and serial sectioning may require thousands of ultrathin sections to obtain several final sections and thus may be impractical. The use of serial ultrathin sections demonstrated that GLUT1 labeling was scattered in different planes of BCECs (Fig. 5c) and that the corresponding fluorescent signal (green, Fig. 5b) extended along Z axis was a summation of multiple GLUT1 signals rather than a representation of point spread function from a molecule [21].

A previous immunoEM study on ultrathin frozen section of rat sciatic nerve demonstrated immunolocalization of GLUT1 along the luminal and abluminal plasma membrane of the endothelial cells [22]. Although the authors' procedure of immunoEM on ultrathin frozen sections is meticulous, it is not yet possible to identify further details of topology of GLUT1 in relation to plasma membranes or intracellular organelle. Similarly, ultrastructural localization of GLUT1 along luminal/abluminal membranes and cytoplasm of BCECs was reported [16]. Although use of detergent and hydrophilic compound (LR white) for embedding facilitated immunolabeling, ultrastructural details were not sufficiently preserved to determine the topological relation of GLUT1 molecules to intracytoplasmic structures or vesicles [6,16–18], which are supposed to participate in glucose transport. Similar localization of GLUT1 molecules was reproduced in our experiment when the anti-GLUT1 antibody was applied at 1:200 (Fig. 4b and e) [4]. It should be noticed that luminal GLUT1 signals are relatively large and protruding into the lumen (Fig. 4e).

At a lower concentration (1:5000), localization of GLUT1 molecules was found at luminal edge of BCEC (Fig. 4f) and in vesicles near the luminal membrane (Fig. 6e and f) or in the cytoplasm (Fig. 6b, arrowhead). Although it is difficult to decide 'optimal' concentration of the primary antibody especially in immunoEM, it is quite sure that lower concentration of antibody (1:5, 000) provides more specific labeling than higher concentration (1:200). Moreover, smaller size of GLUT1 signals at lower concentration (1:5000, Fig. 4c and f) relative to their higher concentration counterpart (1:200, Fig. 4b and e) may be related to enhanced specificity, which is advantageous to immunolocalize small molecules as GLUT1. When the primary antibody was used at a lower concentration (1:5000), only a few numbers of signals were obtained by the method of immunolabeling in this study compared to previous studies. By increasing the primary antibody concentration (1:200) as shown in Fig. 4, it is possible to raise the immune positive signal to the same level as previous reports [4]. GLUT1 signals were localized on intracellular vesicles (Fig. 6b, arrowhead), cellular membrane on the abluminal side of the cell (Fig. 6b and d, arrows) and cellular membrane on the luminal side of the cell (Fig. 6e and f, arrowheads), as well as in medium-sized vesicles (Fig. 6g, arrowhead). We succeeded in showing for the first time GLUT1 molecules clearly on coated vesicles on the plasma membrane and in medium-sized vesicles in the cytosol, suggesting the biological mechanism of GLUT1 taken up into mouse BCECs by coated vesicles. Although ∼40 coated vesicles displayed the GLUT1 signal, while uncoated vesicles did not contain the GLUT1 signal. However, this result alone cannot rule out the presence of uncoated vesicles containing GLUT1. Of the vesicles we observed, ∼40% of the coated vesicles showed the GLUT1 signal, whereas none of the uncoated vesicles showed the GLUT1 signal. However, among the vesicles that we observed, ∼40% of the coated vesicles displayed the GLUT1 signal, whereas none of the uncoated vesicles displayed it. Therefore, our results suggest that GLUT1 in mouse BCECs is internalized via an endocytic pathway that involves mainly coated vesicles from the luminal side and that GLUT1 may be transported to a medium-sized structure surrounded by a membrane or to the abluminal side in order to deliver glucose into the brain.

Concluding remarks

Using light microscopy prior to EM observation, we focused an ROI from the entire mouse brain hemisphere to find a representing typical localization pattern of GLUT1 molecules in BCEC. Also, we applied serial ultrathin sectioning for Z-coordinate adjustment in EM to the CLEM method, and we observed the ultrastructural localization of tiny and scattered molecules of GLUT1 in mouse brain tissue. The GLUT1 molecules were clearly localized on coated vesicles in mouse BCECs. Although further studies are needed, we expect that our findings and newly developed strategy will help to clarify the pathway and physiological and pathological functions of GLUT1.

Author contributions

All authors had full access to all the data in the study and take responsibility for the integrity of the data and the accuracy of the data analysis.

Conceptualization, H.K., T.U. and T.Y.; methodology, A.Y., K.W., A.N., Y.S. and T.U.; investigation, A.Y.; formal analysis, A.Y., K.W. and T.U.; writing—original draft, A.Y.; writing—review & editing, Y.N. and T.U.; visualization, A.Y., Y.N. and T.U.; supervision, T.U. and T.Y.; funding acquisition, Y.N. and T.Y.

Funding

Center of Innovation (COI) Program (Grant Number JPMJCE1305) from the Japan Science and Technology Agency (JST), Japan Agency for Medical Research and Development (AMED) (Grant Number JP20dm0107063), CryoEM Gateway research Support fund from JEOL Ltd. and CeSPIA Inc.

Data accessibility

Data sharing is not applicable to this article.

Conflict of interest

The authors declare that they have no conflict of interest.

References

1. Eyster C A, Higginson J D, Huebner R, Porat-Shiliom N, Weigert R, Wu W W, Shen R F, and Donaldson J G (2009) Discovery of new cargo proteins that enter cells through clathrin-independent endocytosis. *Traffic* 10: 590–599.
2. Anraku Y, Kuwahara H, Fukusato Y, Mizoguchi A, Ishii T, Nitta K, Matsumoto Y, Toh K, Miyata K, Uchida S, Nishina K, Osada K, Itaka K, Nishiyama N, Mizusawa H, Yamasoba T, Yokota T, and Kataoka K (2017) Glycaemic control boosts glucosylated nanocarrier crossing the BBB into the brain. *Nat. Commun.* 8: 1001.
3. Uchida Y, Ohtsuki S, Katsukura Y, Ikeda C, Suzuki T, Kamiie J, and Terasaki T (2011) Quantitative targeted absolute proteomics of human blood-brain barrier transporters and receptors. *J. Neurochem.* 117: 333–345.
4. Farrell C L and Pardridge W M (1991) Ultrastructural localization of blood-brain barrier-specific antibodies using immunogold-silver enhancement techniques. *J. Neurosci. Methods* 37: 103–110.
5. Cornford E M, Hyman S, and Pardridge W M (1993) An electron microscopic immunogold analysis of developmental up-regulation of the blood-brain barrier GLUT1 glucose transporter. *J. Cereb. Blood Flow Metab.* 13: 841–854.
6. Dobrogowska D H and Vorbrodt A W (1999) Quantitative immunocytochemical study of blood-brain barrier glucose transporter (GLUT-1) in four regions of mouse brain. *J. Histochem. Cytochem.* 47: 1021–1030.
7. Riskin A, Nannegari V H, and Mond Y (2008) Acute effectors of GLUT1 glucose transporter subcellular targeting in CIT3 mouse mammary epithelial cells. *Pediatr. Res.* 63: 56–61.
8. Stirling J W (1990) Immuno- and affinity probes for electron microscopy: a review of labeling and preparation techniques. *J. Histochem. Cytochem.* 38: 145–157.
9. Jones J C R (2016) Pre- and post-embedding immunogold labeling of tissue sections. *Methods Mol. Biol.* 1474: 291–307.
10. Tatsumi S, Uchihara T, Aiba I, Iwasaki Y, Mimuro M, Takahashi R, and Yoshida M (2014) Ultrastructural differences in pretangles between Alzheimer disease and corticobasal degeneration revealed by comparative light and electron microscopy. *Acta Neuropathol. Commun.* 2: 1–11.

11. Uematsu M, Nakamura A, Ebashi M, Hirokawa K, Takahashi R, and Uchihara T (2018) Brainstem tau pathology in Alzheimer's disease is characterized by increase of three repeat tau and independent of amyloid β. *Acta Neuropathol. Commun.* 6: 1.
12. Takizawa T, Powell R D, Hainfeld J F, and Robinson J M (2015) FluoroNanogold: an important probe for correlative microscopy. *J. Chem. Biol.* 8: 129–142.
13. Cortese K, Diaspro A, and Tacchetti C (2009) Advanced correlative light/electron microscopy: current methods and new developments using Tokuyasu cryosections. *J. Histochem. Cytochem.* 57: 1103–1112.
14. Winkler E A, Nishida Y, Sagare A P, Rege S V, Bell R D, Perimutter D, Sengillo J D, Hillman S, Kong P, Nelson A R, Sullivan J S, Zhao Z, Meiselman H J, Wendy R B, Soto J, Abel E D, Makshanoff J, Zuniga E, De Vivo D C, and Zlokovic B V (2015) GLUT1 reductions exacerbate Alzheimer's disease vasculo-neuronal dysfunction and degeneration. *Nat. Neurosci.* 18: 521–530.
15. Gerhart D Z, Le Vasseur R J, Broderius M A, and Drewes L R (1989) Glucose transporter localization in brain using light and electron immunocytochemistry. *J. Neurosci. Res.* 22: 464–472.
16. Farrell C L and Pardridge W M (1991) Blood-brain barrier glucose transporter is asymmetrically distributed on brain capillary endothelial lumenal and ablumenal membranes: an electron microscopic immunogold study. *Proc. Natl. Acad. Sci. U. S. A.* 88: 5779–5783.
17. Bolz S, Farrell C L, Dietz K, and Wolburg H (1996) Subcellular distribution of glucose transporter (GLUT-1) during development of the blood-brain barrier in rats. *Cell Tissue Res.* 284: 355–365.
18. Vorbrodt A W, Dobrogowska D H, Tarnawski M, Meeker H C, and Carp R I (2001) Quantitative immunogold study of glucose transporter (GLUT-1) in five brain regions of scrapie-infected mice showing obesity and reduced glucose tolerance. *Acta Neuropathol.* 102: 278–284.
19. Bishop D L, Misgeld T, Walsh M K, Gan W B, and Lichtman J W (2011) Near-infrared branding efficiently correlates light and electron microscopy. *Nat. Methods* 8: 568–570.
20. Salas-Burgos A, Iserovich P, Zuniga F, Vera J C, and Fischbarg J (2004) Predicting the three-dimensional structure of the human facilitative glucose transporter glut1 by a novel evolutionary homology strategy: insights on the molecular mechanism of substrate migration, and binding sites for glucose and inhibitory molecules. *Biophys. J.* 87: 2990–2999.
21. Booth M J, Neil M A A, Juskaitis R, and Wilson T (2002) Adaptive aberration correction in a confocal microscope. *Proc. Natl. Acad. Sci. U. S. A.* 99: 5788–5792.
22. Tserentsoodol N, Shin B C, Koyama H, Suzuki T, and Tanaka K (1999) Immunolocalization of tight junction proteins, occludin and ZO-1, and glucose transporter GLUT1 in the cells of the blood-nerve barrier. *Arch. Histol. Cytol.* 62: 459–469.